Mixed dimensionality of confined conducting electrons tied to ferroelectric surface distortion on an oxide

N. C. Plumb,[1,*] M. Salluzzo,[2] E. Razzoli,[1] M. Månsson,[3,4] M. Falub,[1] J. Krempasky,[1] C. E. Matt,[1] J. Chang,[1,5] M. Schulte,[6] J. Braun,[6] H. Ebert,[6] J. Minár,[6] B. Delley,[7] K.-J. Zhou,[1] T. Schmitt,[1] M. Shi,[1] J. Mesot,[1,4,5] L. Patthey,[1,8] and M. Radović[1,5,8,†]

[1]*Swiss Light Source, Paul Scherrer Institut, CH-5232 Villigen PSI, Switzerland*
[2]*CNR-SPIN, Complesso Universitario Monte S. Angelo, Via Cinthia I-80126, Napoli, Italy*
[3]*Laboratory for Neutron Scattering, Paul Scherrer Institut, CH-5232 Villigen PSI, Switzerland*
[4]*Laboratory for Solid State Physics, ETH Zürich, CH-8093 Zürich, Switzerland*
[5]*Institut de la Matiere Complexe, EPF Lausanne, CH-1015 Lausanne, Switzerland*
[6]*Department Chemie, Ludwig-Maximilians-Universität München, 81377 München, Germany*
[7]*Condensed Matter Theory Group, Paul Scherrer Institut, CH-5232 Villigen PSI, Switzerland*
[8]*SwissFEL, Paul Scherrer Institut, CH-5232 Villigen PSI, Switzerland*

Conducting oxide interfaces have been the subject of intense research due to the technological promise and theoretical challenges they present. The recent discovery of a metallic surface state on $SrTiO_3$ may open an alternate route to simplified low-dimensional oxide conductors and give new insights into interface phenomena, but its origin — particularly as it might relate to oxygen vacancies — has been unclear. Here we show that the surface state consists of non-bulklike 3D Fermi surface (FS) components coexisting with quasi-2D components. Like their more 2D counterparts, the size and character of the 3D components are fixed with respect to the preparation of the bulk sample. Moreover, while it is possible to trigger the metallicity by irradiating the sample surface, the spectroscopic signatures of this electronic reconstruction do not scale with any changes in stoichiometry. The results suggest that the distribution and electronic structure of carriers in the surface region are directly linked to the electrostatic conditions that support a ferroelectric surface distortion. The concept of such a "displacement state" is potentially relevant for a broad class of materials and heterostructures that are close to ferroelectric instabilities at their surfaces or interfaces.

$SrTiO_3$ (STO) is a foundational material for the coming age of multifunctional oxide devices. Perhaps most famously, it hosts an electron gas at its interface with $LaAlO_3$ (LAO) and other related transition metal oxides [1–7] — a behavior that is extremely promising for technological applications [8]. However, STO by itself exhibits rich and complex phenomena such as superconductivity [9] and ferroelectricity [10–13]. Moreover, it was recently shown that a low-dimensional metal can form on the bare surface of STO [14–16]. The discovery promises to extend this material's technological importance, as well as shed new light on the physics of metallic oxide surfaces and interfaces in general, so long as the origin of the state can be understood and harnessed.

Although stoichiometric STO is nominally an insulator with a 3.2-eV bandgap, metallicity in or on STO has been observed by photoemission for many years [17, 18]. However, the electronic structure and low-dimensional nature of the metallic surface state on STO had not been deeply appreciated until very recent angle-resolved photoemission spectroscopy (ARPES) and scanning tunneling spectroscopy (STS) studies [14–16]. While individually the experiments can be interpreted to support the notion that oxygen vacancies drive the formation of the surface state, collectively their observations are difficult to reconcile within this model. On one hand, the metallic state showed robustness to a variety of sample preparations [14], but on the other hand, the sensitivity of its oxygen valence band structure to irradiation in ultra-high vacuum (UHV) [15] seemed to indicate that photo-induced oxygen loss might substantially alter the state. At some point oxygen loss due to annealing can even destroy the surface state [16], which appears to give way to the spectroscopic signatures of a bulklike metallic state [19].

In order to investigate these issues and gain new insights into the nature and origin of the metallic surface, we used ARPES and core level x-ray photoemission spectroscopy (XPS) to study STO(001) wafers that were prepared by a standard etching and annealing process in order to be highly TiO_2-terminated [20]. Just prior to performing the photoemission measurements, the samples underwent various *in situ* annealing procedures in order to clean the surfaces and to either generate or fill oxygen vacancies, thereby changing the nominal doping in the bulk of each sample. In addition, one sample was lightly Nb-doped (0.25% by weight, Nb-STO). The preparations are summarized in Table I.

The ARPES measurements reveal four FS components, which are highlighted in Fig. 1. The data shown come from Nb-STO, but all the samples are virtually identical in terms of the electronic structure at the surface. When measured using a photon energy of $h\nu = 85$ eV, the FS in the surface k_x-k_y plane is made up of two concentric rings (the inner of which has only very weak intensity), as well as two ellipsoids aligned along the k_x and k_y directions (Fig. 1a). At other photon energies, the ellipsoids vanish while the rings remain, as demonstrated at $h\nu = 51$ eV

(Fig. 1b). Based on their k_x-k_y symmetry, the ellipsoids can be associated with Ti $3d_{xz}$ / $3d_{yz}$ orbitals and the rings with Ti $3d_{xy}$ orbitals. The inner ring may be a quantum well subband of the outer ring [14, 15] (i.e., the $n = 2$ quantum well state, while the outer ring is $n = 1$), but so far one cannot rule out that it comes from the second (i.e., subsurface) TiO_2 layer [21], or even some more exotic mechanism. The rings had already been considered within the context of the surface metallic state [14, 15], but until now the ellipsoids had never been fully characterized and were even proposed to be bulk states [22].

The different photon energies used to probe the FS in the k_x-k_y plane correspond to different planes cutting across the k_z axis. By varying the photon energy, we mapped the complete FS in 3D. Figure 1e shows the structure of the FS evaluated as a function of $\boldsymbol{k} = (k_x, 0, k_z)$. The outer ring has nearly perfect 2D character, with only a slight deviation in the Fermi momentum k_F near the Brillouin zone boundary at $k_z = 5\ \pi/a$. The character of the inner ring is somewhat less 2D-like; it is highly cylindrical with long parallel segments, but near the zone boundaries along k_z, it appears to close to form "endcaps" of a pill-shaped FS. This behavior can be consistent with spectroscopic enhancement of finely-spaced quantum well states approaching a k_z continuum [23], but firmly establishing such details will require further study. Most interestingly, the $3d_{xz}$ and $3d_{yz}$ bands, which in bulk calculations [18, 22] are expected to be prolate spheroids ("cigars", Fig. 1f), are actually stretched along the k_z axis ("flying saucers", Fig. 1g). The strong elongation of the $3d_{xz}/3d_{yz}$ bands in k_z corresponds to a high effective mass in the out-of-plane direction ($m_z^* \approx 15m_e$), indicating these electrons experience substantial confinement perpendicular to the surface. Crucially, though, the confinement is relaxed enough that these states, while distinct from truly bulk-like electrons, nevertheless show 3D character by virtue of their fully closed Fermi surface components along all $\boldsymbol{k}$ directions. We thus conclude that the $3d_{xz}$ and $3d_{yz}$ electrons penetrate multiple unit cells toward the bulk, while the $3d_{xy}$ electrons are more tightly confined to the surface. The overall picture is supported by quantum well simulations that implied that the confinement potential extends relatively far from the surface [15], and it bears qualitative similarity to the predicted orbital-resolved distribution of carriers in STO near the LAO/STO(001) interface [24].

Like the quasi-2D rings [14], the sizes of the ellipsoids are universal with respect to bulk oxygen vacancies or dopants, further confirming that they are associated with the near-surface region, despite their 3D nature. This is illustrated in Fig. 2a–d, which shows FS's measured on STO samples prepared by various *in situ* annealing treatments summarized in Table I. Based on the measurements in Fig. 1e, the carrier density corresponding to each ellipsoid is roughly 0.01 e^- per 3D unit cell ($\sim 2 \times 10^{20}$ cm^{-3}).

Exposing STO to synchrotron radiation under UHV conditions ($\sim 10^{-11}$ mbar) typical for ARPES can lead to the formation of the metallic surface state [15]. We have closely monitored the electronic and chemical nature of this process via valence band photoemission and core XPS, respectively. In Fig. 2e, starting from an insulating, nominally stoichiometric sample (the same as in Fig. 2a) that initially shows no FS, we exposed the sample to the beam for an initial time t_0 (~ 10 minutes using $h\nu = 47$ eV) to establish the onset of surface metallicity. Once this weak conductivity was present, the sample could be studied without complications due to charging. During the beam exposure, the spectral weight associated with the O $2p$ valence band steadily decreases while a new feature grows inside the bandgap of the bulk insulating STO. These changes coincide with the emergence and intensification of the signal at E_F, which is (meta)stable for hours under UHV conditions, even when no beam is being applied (also noted in [15]).

As mentioned earlier, similar observations had prompted suspicion that photons could cause the surface to become doped by inducing oxygen vacancies [15]. However, core level measurements, which are more reliable for quantitative surface chemistry, paint a different picture. Figs. 2f–h show XPS of the Ti $2p$, O $1s$, and Sr $3d$ core levels as a function of irradiation time. The spectra were taken at nominal t_0 (established at a newly exposed spot) and later, at t_f, after a dose of 47-eV photons approximately equivalent to the 1 hour of irradiation in Fig. 2e. In the Ti $2p$ spectra (Fig. 2f), weight is transferred from the Ti^{4+} peaks to shoulders at lower binding energy. Adopting the conventional nomenclature, these are signatures of "Ti^{3+}" states, although we will soon argue that, strictly speaking, they arise from partial electron transfer due to enhanced Ti-O covalency and are therefore more properly thought of as $Ti^{3+\delta(z)}$. The Ti^{3+} states are concentrated near the surface, which we have confirmed by the spectrum's emission angle dependence (see Supplimentary Information). In addition to the changes in the Ti $2p$ features, all the XPS spectra become asymmetrically distorted by transferring weight to the high binding energy sides of the peaks, which is a well-known effect of photohole screening in the metallic state [25]. However, despite these changes in the XPS lineshapes, the estimated total spectral weight at t_0 and t_f (I_0 and I_f, respectively) associated with each core level is conserved to within a few percent. Particular importance should be given to the conservation of Sr $3d$ spectral weight, because the background and lineshape of this doublet are much simpler than those of Ti $2p$ and O $1s$, making it more suitable for quantitative analysis. Moreover, Sr resides only in the layers below the TiO_2-terminated surface; due to the shallow probing depth of photoemission techniques [26], its intensity is very sensi-

tive to atoms being lost from the TiO_2 top layer. Notably, total Sr $3d$ spectral weight is conserved to within about 1%.

During the spectral weight transfer process that occurs due to photon irradiation, the FS quickly saturates to a steady volume, while the signal intensity at the Fermi level continues to grow. This is demonstrated in Fig. 2i, which compares total counts near the Fermi level (integrated within a single E-vs.-k_x slice through $k_y = 0$ from -200 meV up to E_F) on the left axis with the total FS volume of the $3d_{xy}$ rings on the right axis as a function of time. The result indicates that impinging photons do not add carriers beyond a certain concentration; they merely enable an increasingly large area of the sample surface to become metallic at a uniformly fixed carrier density, thus brightening the signal seen at the Fermi level.

While very dilute defects such as oxygen vacancies cannot be ruled out (and may play some role in the formation of the metallic state), the profound contrast in scaling between the changes in the near-E_F spectral weight and the relative stability of both the FS and the surface chemistry indicates some other, more fundamental, mechanism is ultimately responsible for the existence and universality of the low-dimensional metallic state. We propose that the metallicity is intimately connected to a ferroelectric distortion in the surface region of STO, which may be triggered, e.g., by irradiating the sample in UHV. An out-of-plane buckling distortion on the surface of STO(001) has been established by many experiments [11, 27–29] and numerical studies [30–34], consistent with the finding that STO exhibits (incipient) ferroelectric behavior [10, 12, 13]. The experiments have emphasized the pronounced buckling ($\lesssim 0.1$ ï¿œ) in the top surface layer, but the calculations generally reveal that additional, weak intralayer Ti-O and Sr-O buckling should extend multiple unit cells from the surface.

Figure 3 illustrates how the basic spectroscopic signatures correlated with the emergence of the surface metallic state can be understood on the basis of the distortion. Often the Ti^{3+} XPS shoulder is thought to indicate the presence of oxygen vacancies, and the in-gap electrons are attributed to associated impurity states [17, 18, 29]. While this view may be appropriate in certain cases, the results here clearly require a different interpretation. Instead, we point out that Ti-O buckling, qualitatively sketched in Fig. 3a, is expected to transfer electron density from O toward Ti due to enhanced covalency [33, 35], which can explain the $Ti^{4+} \rightarrow Ti^{3+}$ transition seen in Fig. 2f. Furthermore, it has been suggested that the surface buckling may be connected to the existence of in-gap spectral weight [36]. To test these possibilities, we compared numerical calculations of the electronic structure of relaxed (i.e., surfaced buckled) and unrelaxed (i.e., truncated bulk) defect-free STO slabs. As expected, the buckling shifts the $2p$ core level peaks of the Ti atoms in the top layer (those most visible to XPS) toward lower binding energy (Fig. 3b). Meanwhile, the $1s$ energy of the top-layer O atoms remains essentially fixed (Fig. 3c). Both behaviors are qualitatively consistent with the experimental results in Figs. 2f and 2g. In addition, Fig. 3d demonstrates that, compared to the unrelaxed slab, the total density of states (DOS) of the relaxed system exhibits a small extra bump $\sim$ 1 eV below E_F, similar to the energy range of the in-gap states highlighted in Fig. 2e. By comparing the layer-resolved local density of states (LDOS) of oxygen in the TiO_2 layers for both slabs, we find that these states originate from oxygen and arise due to broken symmetry. That is, they are already present in the unrelaxed slab, where they are enhanced approaching the surface, but they protrude even further into the gap when the relaxation is taken into account. This finding is consistent with the layer-resolved LDOS previously studied for buckled STO alone[31]. Thus the calculations suggest that the in-gap states can be formed or enhanced due to the extra symmetry-breaking of the ferroelectric distortion.

The real issue that remains is whether the distortion can account for the universal metallic electronic structure of the surface. The buckled layers in the surface region of STO carry dipole moments that establish a gradient in the polarization density $P(z)$ — or equivalently, a gradient in the electric displacement field $D(z)$. Recently, Stengel proposed that $\boldsymbol{D}$ should be regarded as a *microscopic* parameter in certain electrostatically doped semiconductors, including oxides such as STO, where "free charge" should be interpreted as electrons in the conduction band [37]. In such cases, one can draw a parallel with macroscopic electrostatics where a distributed carrier density $n(z)$ and a displacement gradient are fundamentally linked (in 1D) via

$$\frac{dD(z)}{dz} = n(z). \tag{1}$$

Figures 4a–c show an example of a carrier distribution simulation based on the *ab initio* D-response curves of the dielectric properties of STO calculated by Stengel. In creating any reasonable simulation, three constraints come into play: (i) the carrier concentration at the surface is ≈ 0.14 e^-/a^3 (the total 3D unit cell average combining both types of FS components); (ii) the band bending at the surface must be at least -230 meV relative to the bulk (i.e., the depth of the outer ring dispersion); and (iii) the measured $3d_{xy}$–$3d_{xz}/3d_{yz}$ splitting implies that the surface displacement $D(z = 0)$ is roughly -0.2 to -0.3 e^-/a^2 [37]. One finds that a simple "2D" form of $n(z)$, such as a narrow wedge or single exponential, is necessary but not sufficient to satisfy (i)–(iii). This is because $D(z)$ must ramp quickly to satisfy conditions (i) and (iii) via Eq. (1), but in doing so the resulting band bending is far too small to be consistent with condition (ii). However, adding a second, relatively flat

charge distribution extending over many unit cells can contribute significant band bending to yield reasonable results. In light of our ARPES measurements, we naturally associate the more highly confined component of the carrier distribution with the quasi-2D $3d_{xy}$ rings and the deeper carrier distribution with the 3D $3d_{xz}/3d_{yz}$ ellipsoids (Fig. 4a). This simple model suggests that the two FS components work in concert to stabilize the distortion; the strong buckling in the topmost layer corresponds with the more 2D carrier profile of the $3d_{xy}$ rings in the maximally buckled TiO_2 surface layer, but the band bending necessary to realize this carrier density at the surface (Fig. 4b) comes from the slow buildup of $D(z)$ (Fig. 4c) originating from weaker buckling deeper in the sample and corresponding with the carrier distribution of the $3d_{xz}/3d_{yz}$ ellipses. Thus the mixed dimensionality of the surface state appears to be critical to understanding its origin, and the important role played by the deeply penetrating $3d_{xz}/3d_{yz}$ states may explain why standard slab calculations of only a few unit cells fail to predict metallicity while qualitatively capturing other aspects of the structural and electronic changes at the surface.

As for the actual source of the carriers, again the electrostatic considerations offer an explanation. The negative charge in the conducting near-surface region should be balanced by an infinitessimally thin positive charge density at the surface equal to $D(0)$, leaving the sample neutral as a whole. This would suggest that electrons are depleted from the valence band of the buckled surface oxygen (in this case by photoexcitation) and distributed into titanium conduction band states in the subsurface where they become less visible to the photoemission experiment. The overall picture fits nicely with the decrease in valence band intensity seen in Fig. 2e and, as already discussed, with the photo-induced Ti $2p$ core level shift in Fig.2f.

The electrostatic model lends intuition to the universal pinning of the FS on STO; the system most likely has a strong energetic preference for a particular range of distortions [34], but any feasible distortion pattern must also give rise to band bending such that $n(z)$ has the correct form to satisfy Eq. (1). Once realized — perhaps via a trigger such as photons, field effect, disorder, strain, etc. — the electronic structure of the metallic state is effectively locked, with the carriers and distortion stabilizing each other. Such "displacement states" are likely to be general phenomena on a broad class of transition metal oxide surfaces where confined ferroelectricity can arise, possibly explaining the recent observation of a very similar state on $KTaO_3$ [38], as well as surface conductivity on poled ferroelectric $BaTiO_3$ [39–41]. They could also play a crucial role, e.g., in resistive switching behavior [42] and may be connected to conductivity at oxide interfaces [1], including surprising systems [4–7] where the polar catastrophe model [43] does not apply. In those cases, one can imagine that a very thinly deposited overlayer neutralizes the ferroelectric distortion by restoring 6-fold coordination to the surface Ti atoms. Above some critical thickness of the overlayer, however, the accumulated strain and/or defects trigger a distortion near the interface [6], giving rise to a displacement gradient and its accompanying carrier electrons. Over time it should become possible to predict, create, and manipulate novel displacement states, thereby opening new avenues in the design of multifunctional oxide devices.

* nicholas.plumb@psi.ch
† milan.radovic@psi.ch

[1] Ohtomo, A. & Hwang, H. Y. A high-mobility electron gas at the $LaAlO_3/SrTiO_3$ heterointerface. *Nature* **427**, 423–426 (2004).

[2] Hotta, Y., Susaki, T. & Hwang, H. Y. Polar discontinuity doping of the $LaVO_3/SrTiO_3$ interface. *Phys. Rev. Lett.* **99**, 236805 (2007).

[3] Perna, P. *et al.* Conducting interfaces between band insulating oxides: The $LaGaO_3/SrTiO_3$ heterostructure. *Appl. Phys. Lett.* **97**, 152111 (2010).

[4] Chen, Y. *et al.* Metallic and insulating interfaces of amorphous $SrTiO_3$-based oxide heterostructures. *Nano Lett.* **11**, 3774–3778 (2011).

[5] Herranz, G., Sánchez, F., Dix, N., Scigaj, M. & Fontcuberta, J. High mobility conduction at (110) and (111) $LaAlO_3/SrTiO_3$ interfaces. *Sci. Rep.* **2**, 758 (2012).

[6] Annadi, A. *et al.* Unexpected Anisotropic Two Dimensional Electron Gas at the LaAlO3/SrTiO3 (110) Interface. *ArXiv e-prints* (2012). URL `http://arxiv.org/abs/1208.6135`. 1208.6135.

[7] Chen, Y. Z. *et al.* A high-mobility two-dimensional electron gas at the spinel/perovskite interface of γ-$Al_2O_3/SrTiO_3$. *Nat. Commun.* **4**, 1371 (2013).

[8] Mannhart, J. & Schlom, D. G. Oxide interfaces — an opportunity for electronics. *Science* **327**, 1607–1611 (2010).

[9] Schooley, J. F., Hosler, W. R. & Cohen, M. L. Superconductivity in semiconducting $SrTiO_3$. *Phys. Rev. Lett.* **12**, 474–475 (1964).

[10] Bednorz, J. G. & Müller, K. A. $Sr_{1-x}Ca_xTiO_3$: An XY quantum ferroelectric with transition to randomness. *Phys. Rev. Lett.* **52**, 2289–2292 (1984).

[11] Bickel, N., Schmidt, G., Heinz, K. & Müller, K. Ferroelectric relaxation of the $SrTiO_3$ (100) surface. *Phys. Rev. Lett.* **62**, 2009–2011 (1989).

[12] Kim, Y. S. *et al.* Observation of room-temperature ferroelectricity in tetragonal strontium titanate thin films on $SrTiO_3$ (001) substrates. *Appl. Phys. Lett.* **91**, 042908 (2007).

[13] Jang, H. W. *et al.* Ferroelectricity in strain-free $SrTiO_3$ thin films. *Phys. Rev. Lett.* **104**, 197601 (2010).

[14] Santander-Syro, A. F. *et al.* Two-dimensional electron gas with universal subbands at the surface of $SrTiO_3$. *Nature* **469**, 189–193 (2011).

[15] Meevasana, W. *et al.* Creation and control of a two-dimensional electron liquid at the bare $SrTiO_3$ surface. *Nature Mater.* **10**, 114–118 (2011).

[16] Di Capua, R. *et al.* Observation of a two-dimensional electron gas at the surface of annealed $SrTiO_3$ single crys-

tals by scanning tunneling spectroscopy. *Phys. Rev. B* **86**, 155425 (2012).

[17] Courths, R., Cord, B. & Saalfeld, H. Bulk and surface Ti3*d* valence and defect states in $SrTiO_3$ (001) from resonant photoemission. *Solid State Commun.* **70**, 1047–1051 (1989).

[18] Aiura, Y. *et al.* Photoemission study of the metallic state of lightly electron-doped $SrTiO_3$. *Surf. Sci.* **515**, 61–74 (2002).

[19] Chang, Y. J., Bostwick, A., Kim, Y. S., Horn, K. & Rotenberg, E. Structure and correlation effects in semiconducting $SrTiO_3$. *Phys. Rev. B* **81**, 235109 (2010).

[20] Kawasaki, M. *et al.* Atomic control of the $SrTiO_3$ crystal surface. *Science* **266**, 1540–1542 (1994).

[21] Popović, Z. S., Satpathy, S. & Martin, R. M. Origin of the two-dimensional electron gas carrier density at the $LaAlO_3$ on $SrTiO_3$ interface. *Phys. Rev. Lett.* **101**, 256801 (2008).

[22] Meevasana, W. *et al.* Strong energy-momentum dispersion of phonon-dressed carriers in the lightly doped band insulator $SrTiO_3$. *New J. Phys.* **12**, 023004 (2010).

[23] Ohta, T. *et al.* Interlayer interaction and electronic screening in multilayer graphene investigated with angle-resolved photoemission spectroscopy. *Phys. Rev. Lett.* **98**, 206802 (2007).

[24] Delugas, P. *et al.* Spontaneous 2-dimensional carrier confinement at the *n*-type $SrTiO_3/LaAlO_3$ interface. *Phys. Rev. Lett.* **106**, 166807 (2011).

[25] Doniach, S. & Šunjić, M. Many-electron singularity in x-ray photoemission and x-ray line spectra from metals. *J. Phys. C* **3**, 285–291 (1970).

[26] Seah, M. P. & Dench, W. A. Quantitative electron spectroscopy of surfaces: A standard data base for electron inelastic mean free paths in solids. *Surf. Interface Anal.* **1**, 2–11 (1979).

[27] Hikita, T., Hanada, T., Kudo, M. & Kawai, M. Structure and electronic state of the TiO_2 and SrO terminated $SrTiO_3$(100) surfaces. *Surf. Sci.* **287–288**, 377–381 (1993).

[28] Ikeda, A., Nishimura, T., Morishita, T. & Kido, Y. Surface relaxation and rumpling of TiO_2-terminated $SrTiO_3$(001) determined by medium energy ion scattering. *Surf. Sci.* **433–435**, 520–524 (1999).

[29] van der Heide, P., Jiang, Q., Kim, Y. & Rabalais, J. X-ray photoelectron spectroscopic and ion scattering study of the $SrTiO_3$(0 0 1) surface. *Surf. Sci.* **473**, 59–70 (2001).

[30] Padilla, J. & Vanderbilt, D. Ab initio study of $SrTiO_3$ surfaces. *Surf. Sci.* **418**, 64–70 (1998).

[31] Li, Z.-Q., Zhu, J.-L., Wu, C. Q., Tang, Z. & Kawazoe, Y. Relaxations of TiO_2- and SrO-terminated $SrTiO_3$ (001) surfaces. *Phys. Rev. B* **58**, 8075–8078 (1998).

[32] Cheng, C., Kunc, K. & Lee, M. H. Structural relaxation and longitudinal dipole moment of $SrTiO_3(001)(1 \times 1)$ surfaces. *Phys. Rev. B* **62**, 10409–10418 (2000).

[33] Heifets, E., Eglitis, R., Kotomin, E., Maier, J. & Borstel, G. First-principles calculations for $SrTiO_3$(100) surface structure. *Surf. Sci.* **513**, 211–220 (2002).

[34] Eglitis, R. I. & Vanderbilt, D. First-principles calculations of atomic and electronic structure of $SrTiO_3$ (001) and (011) surfaces. *Phys. Rev. B* **77**, 195408 (2008).

[35] Cohen, R. E. Origin of ferroelectricity in perovskite oxides. *Nature* **358**, 136–138 (1992).

[36] Mizokawa, T. *et al.* Photo-induced in-gap states in $SrTiO_3$ probed by photoemission spectroscopy under ultraviolet illumination. *J. Phys. Soc. Jpn.* **79**, 044703 (2010).

[37] Stengel, M. First-principles modeling of electrostatically doped perovskite systems. *Phys. Rev. Lett.* **106**, 136803 (2011).

[38] King, P. D. C. *et al.* Subband structure of a two-dimensional electron gas formed at the polar surface of the strong spin-orbit perovskite $KTaO_3$. *Phys. Rev. Lett.* **108**, 117602 (2012).

[39] Urakami, Y., Yamato, M. & Watanabe, Y. Surface conduction on poled $BaTiO_3$ single crystals in ultra high vacuum. *Ferroelectrics* **346**, 32–36 (2007).

[40] Watanabe, Y., Kaku, S., Matsumoto, D., Urakami, Y. & Cheong, S. W. Investigation of clean ferroelectric surface in ultra high vacuum (UHV): Surface conduction and scanning probe microscopy in UHV. *Ferroelectrics* **379**, 157–167 (2009).

[41] Fechner, M., Ostanin, S. & Mertig, I. Effect of the surface polarization in polar perovskites studied from first principles. *Phys. Rev. B* **77**, 094112 (2008).

[42] Szot, K., Speier, W., Bihlmayer, G. & Waser, R. Switching the electrical resistance of individual dislocations in single-crystalline $SrTiO_3$. *Nature Mater.* **5**, 312–320 (2006).

[43] Nakagawa, N., Hwang, H. Y. & Muller, D. A. Why some interfaces cannot be sharp. *Nature Mater.* **5**, 204–209 (2006).

Acknowledgements

Experiments were carried out at the Surface/Interface Spectroscopy (SIS, X09-LA) beamline at the Swiss Light Source. We are grateful for valuable conversations with J. H. Dil, V. N. Strocov, M. Kobayashi, C. Quitmann, C. Monney, A. Uldry, F. Baumberger, A. F. Santander-Syro, F. Fortuna, C. Bareille, E. Rotenberg, L. Moreschini, Y. J. Chang, C. W. Schneider, P. R. Willmott, C. Cancellieri, M. Reinle-Schmitt, R. Claessen, and F. Miletto Granozio. M. Kopf and M. Horisberger lent technical assistance. M. M. was partly supported by the Swedish Foundation BLANCEFLOR Boncompagni-Ludovisi nï¿œe Bildt. M. F. acknowledges financial support from the Swiss National Science Foundation (Project-No PMPDP2_128995). M. Schulte, J. B., H. E., and J. Minï¿œr acknowledge financial support from the Deutsche Forschungsgemeinschaft (FOR 1346) and the Bundesministerium fi¿œr Bildung und Forschung (05K10WMA). C. M. was partially supported by the Swiss National Science Foundation and its NCCR MaNEP.

Author contributions

N. C. P. performed the data analysis and wrote the paper under the supervision of M. R. and with valuable input from all the coauthors, including J. C., J. Mesot, and M. Shi. N. C. P., M. R., M. Salluzzo, E. R., M. M., M. F., J. K., and C. E. M. collected photoemission data. N. C. P. made the electrostatic simulations in close consultation with M. R. and M. Salluzzo. M. Salluzzo studied the sample surfaces by AFM and STM. M. Schulte, J. B., H. E., J. Minï¿œr, and B. D. performed calculations. K.-J. Z. and T. S. shared crucial insights,

analysis, and expertise gained from parallel experiments performed within the group at Paul Scherrer Institut. M. R. and L. P. conceived the project.

Additional information

The authors declare no competing financial interests.

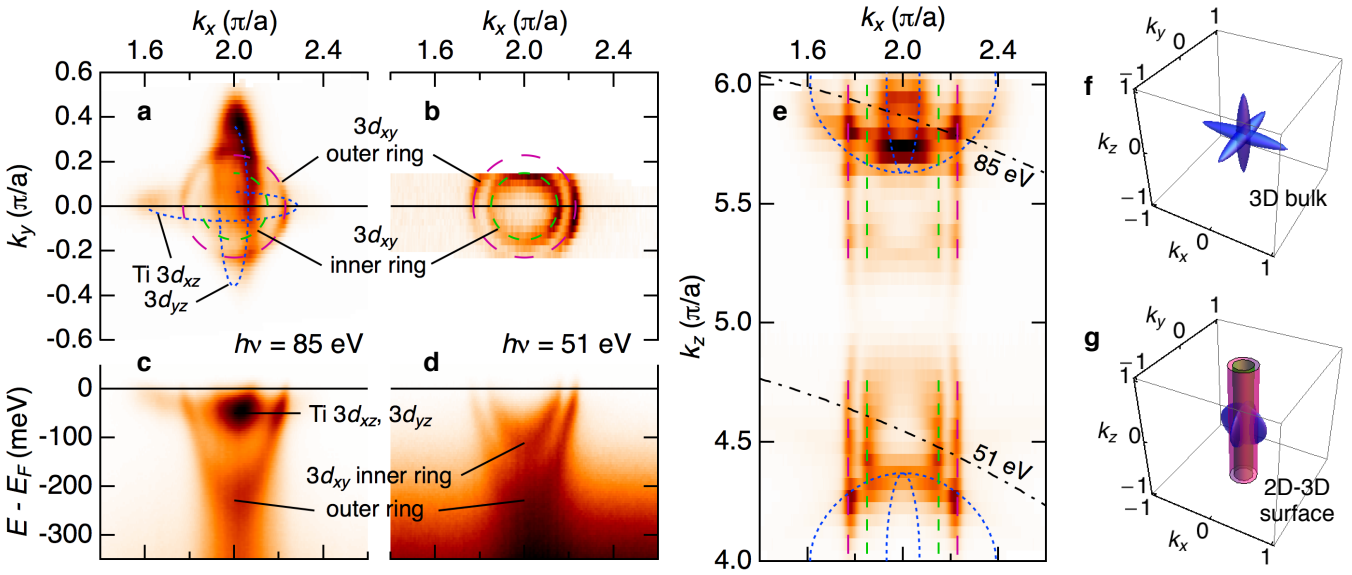

Figure 1 | Three-dimensional view of the near-E_F electronic structure of the metallic surface region on STO. a, Fermi surface map in the k_x-k_y plane measured at $h\nu = 85$ eV. The data are from the Brillouin zone centered at $(k_x, k_y) = (2\pi/a, 0)$. The ellipsoidal Ti $3d_{xz}$ and $3d_{yz}$ bands are illustrated by dotted blue lines, while the Ti $3d_{xy}$ inner and outer rings are highlighted by short-dashed green lines and long-dashed magenta lines, respectively. **b,** Analogous data taken at $h\nu = 51$ eV. **c, d,** Band dispersions along $(k_x, k_y = 0)$ for each of the above panels. **e,** Fermi surface cut in the k_x-k_y plane at $k_y = 0$. The dot-dashed lines indicate the curvature of Fermi surface cuts in **a** and **b**. **f,** Expected shape of the 3D Fermi surface in the bulk. For reference, the FS volume shown here corresponds to a carrier density of about 4×10^{20} cm^{-3}. **g,** Simplified representation of the mixed quasi-2D and 3D Fermi surface sheets at the STO surface. The colors correspond with the lines in **a–b**.

Table I | *In situ* preparation procedures for the samples in Fig. 2a–d.

Fig. 2	Sample	Environment	T (°C)	t (h)	Color	Description
a	STO	O_2, 100 mbar	550	2	Clear	nominally stoichiometric
b	STO	UHV, $\sim 10^{-9}$ mbar	300	15	Clear	"low" oxygen vacancies
c	STO	UHV, $\sim 10^{-9}$ mbar	720	1	Black	"high" oxygen vacancies
d	Nb-STO	O_2, 100 mbar	550	2	Black	lightly Nb-doped

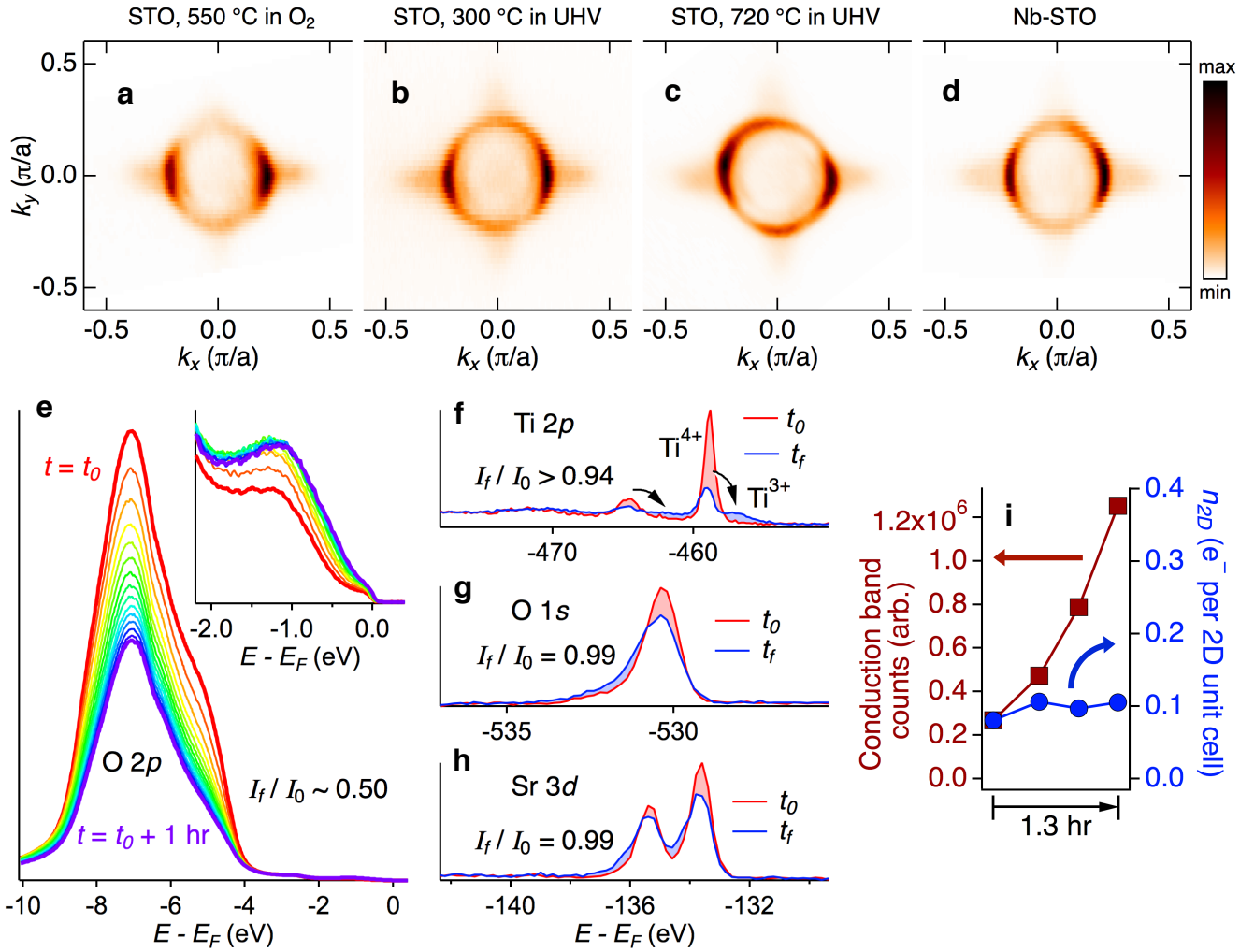

Figure 2 | Universality of the Fermi surface with respect to annealing conditions and photo-induced changes. a–d, Fermi surfaces of the STO samples described in Table I. The measurements were performed in the first Brillouin zone using $h\nu = 85$ eV. **e**, Study of the oxygen valence band spectrum of the sample in **a** as a function of irradiation time. The inset shows in-gap states that form while the main valence band intensity decreases. **f–h**, XPS spectra for Ti $2p$, O $1s$ and Sr $3d$ core levels measured before (t_0) and after (t_f) a similar radiation dose as in **e**. **i**, Comparison of the time evolution of total integrated counts in the conduction band region and the combined 2D carrier density of the inner and outer $3d_{xy}$ ring-shaped FS components.

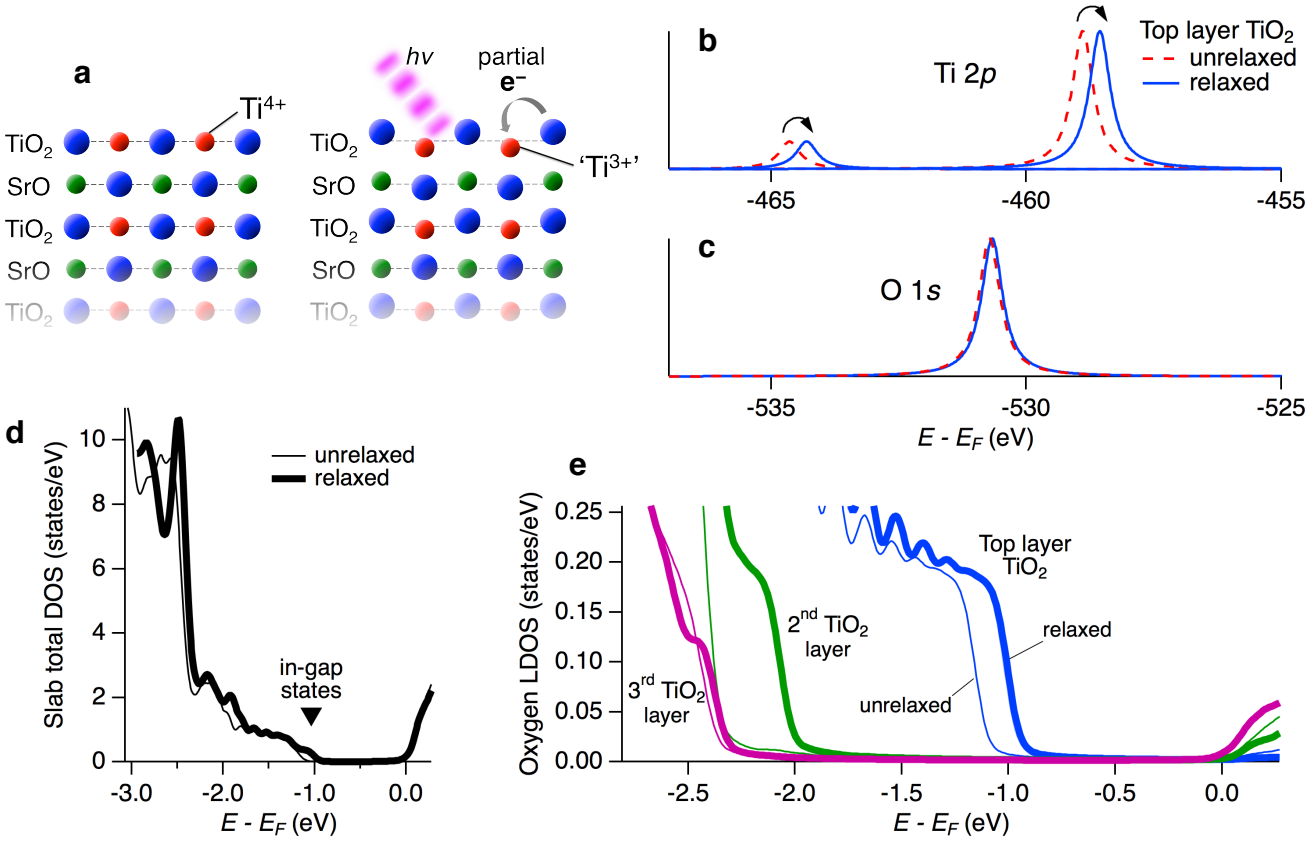

Figure 3 | Spectroscopic signatures of ferroelectric surface distortion. **a**, Qualitative sketch of the photo-assisted surface relaxation of STO and corresponding $Ti^{4+} \rightarrow Ti^{3+}$ charge redistribution. **b, c,** Calculated shifts of the Ti $2p$ and O $1s$ core level peaks in the top TiO_2 layer of the relaxed STO surface relative to the unrelaxed surface. **d,** Comparison of the total DOS of the relaxed and unrelaxedSTO slabs. **e,** Layer-resolved LDOS of oxygen for the relaxed (thick lines) and unrelaxed (thin lines) structures.

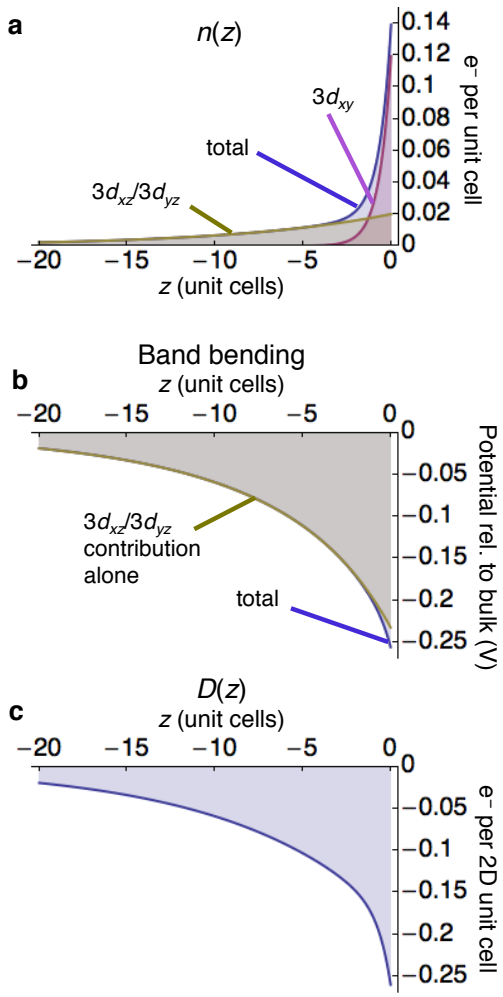

Figure 4 | Electrostatic simulation of carriers in the surface region of STO. a, Sketch of a proposed carrier distribution matching the surface ($z = 0$) carrier densities of the $3d_{xy}$ ring-shaped and $3d_{xz}/3d_{yz}$ ellipsoidal FS components and consistent with their quasi-2D and 3D characters, respectively. Using recent calulations [37], the carrier distribution in **a** corresponds with the band bending in **b**, which is sufficient to explain the depth of the conduction band dispersions shown in Fig. 1. **c,** The carrier distribution is equivalent to a gradient in the electric displacement arising from the surface distortion.